The 28th Annual International Pittsburgh Coal Conference, Pittsburgh, PA, USA, September 12 - 15, 2011
Paper 32-2

NUMERICAL ANALYSIS OF GASIFICATION PERFORMANCE VIA FINITE-RATE MODEL IN A CROSS-TYPE TWO-STAGE GASIFIER

Yan-Tsan Luan and Yau-Pin Chyou*
Nuclear Fuels and Materials Division
Institute of Nuclear Energy Research
Atomic Energy Council
Longtan, Taoyuan, Taiwan (R.O.C.)

Ting Wang
Energy Conversion & Conservation Center
University of New Orleans
New Orleans, Louisiana 70148, USA

ABSTRACT

The gasification process of a pressurized, oxygen-blown, entrained-flow E-Gas like gasifier through numerical modeling is investigated in this paper by using the commercial software, ANSYS/FLUENT. The 3-D, steady-state Navier-Stokes equations are solved using the Eulerian-Lagrangian method. Coal particles are treated as a discrete phase dispersed in the continuous phase with the stochastic tracking method. Eight species transport reactions consisting of combustion, gasification, volatiles-cracking, and water-gas-shift reaction with assigned chemical reaction rate constants are solved through the Finite-Rate/Eddy-Dissipation Model.

This paper investigates the effects of the O_2/Coal ratio, coal slurry concentration, and 1^{st}-2^{nd} stage fuel distribution ratio on gasification performance, which is evaluated using the outlet species composition, syngas heating value, and cold gas efficiency. The preliminary gasification process is successfully modeled and the global chemical reactions are proved to be strongly affected by the finite rates. The study of varying operating parameters shows that the increasing O_2/Coal ratio results in a decrease of CO, but an increase of CO_2 and exit temperature. With a modified water-gas-shift reaction rate, a more reasonable trend is obtained. As the coal slurry concentration increases, the mass flow rate of H_2, CO_2, and H_2O increase while that of CO decreases. As the amount of coal slurry mass flow in the first stage increases, the exit temperature and the mole concentration of H_2 and CO_2 increase, while the mole concentration of CO decreases. However, because the space inside the E-Gas gasifier is large enough to allow for complete reactions, different fuel distributions do not provide notable influence on gasification performance. The overall results show that the present CFD and reaction models can adequately capture the gasification behavior inside the gasifier. However, further efforts should be made to achieve more precise prediction and advanced analyses in the future.

Key words: coal gasification, CFD modeling, entrained-flow gasifier, E-Gas Gasifier

1. INTRODUCTION

Background

Due to the use of fossil fuel to generate power, large amounts of greenhouse gases are discharged by burning fossil fuels, which is deemed as one of the major causes of global warming. This issue has raised concerns around the world and has lead to a series of international summits to seek solutions to reduce emissions and eventually alleviate global warming and associated issues. There are many ways to reduce carbon emissions. Although technologies for employing renewable energy such as solar, wind, ocean, hydro, and biomass have been developed and been growing at a fast pace, the advantage of utilizing fossil fuels for providing the most affordable electrical energy cannot be replaced overnight by any other technologies today. Among them, coal, which contributes a major amount of CO_2, is still one of the most abundant fossil fuels remaining on earth. According to BP's report [1], the supply of coal will last for at least 119 years.

In Taiwan, a country without domestic coal production, there is still about 34% of energy consumption that comes from coal-fired power plants, in which, 77.62% are for power generation, 1.29% are blast furnaces, 8.52% are for coke production, and 12.58% are for industrial and other purposes [2]. Considering the fact that coal-fired power generation will continue to be the main source of electric power in Taiwan as well as worldwide in the next few decades, the importance of utilizing coal in a cleaner way becomes an urgent issue needed to be addressed immediately. Therefore, it is essential to improve the efficiency of coal combustion or to develop new technologies such as coal gasification as one of the most promising and important technologies that can extend the usability of coal more cleanly and efficiently.

The Institute of Nuclear Energy Research (INER) has devoted themselves to the development of clean coal technology, and plan to build a demonstration gasification facility within next few years. To help understand the gasification process in entrained flow gasifiers and guide the design of the experimental gasifier, developing Computational Fluid Dynamics (CFD) models is considered an important step to enrich INER's research team's knowledge and capability.

During the development of a gasification model of this research team, an intermediate step was undertaken last year by applying the "instantaneous gasification model" to the heterogeneous reactions by assuming that the carbon solid is instantaneously gasified, and the reaction rate of each reaction is determined by the turbulence eddies via the eddy-dissipation model [3, 4]. The **main objective** of this paper is to replace the previous instantaneous gasification model with the more realistic heterogeneous finite-rate reactions using the discrete phase model (DPM) to track each coal particle. The **second objective** is to examine and improve the understanding of the gasifier thermal-flow behavior and gasification process in the uniquely designed E-Gas gasifier.

*Corresponding author (e-mail: ypchyou@iner.gov.tw)

The ultimate goal is to use the developed CFD modeling capability and the knowledge gained during parametric gasification analyses to design and establish a demonstration facility in INER.

Literature Review

In 1979 Wen et al. [5] investigated the Texaco down-draft entrainment pilot plant gasifier through their mathematical model and assessed the influences of the input operating parameters. They concluded that: (1) an increase of oxygen/fuel ratio significantly increases the carbon conversion, resulting in slightly decreased H_2 concentration and increased CO concentration in the product gas; (2) an increase in the steam/fuel ratio increases the H_2 and CO_2 concentration, but decreases the CO concentration; (3) an increase in the operating pressure can increase the degree of carbon conversion particularly at high steam/fuel ratios; and (4) small fuel particles cause higher carbon conversion efficiencies for a given mass feed rate.

Smoot [6] and Eaton et al. [7] comprehensively reviewed the development of coal combustion modeling in fixed, fluidized, and entrained beds respectively. In addition, Smoot and Smith [8] and Hill and Smoot [9] developed a two-dimensional (PGCG-2) and three-dimensional (PGCG-3) pulverized coal combustion model at Brigham Young University. The model solved the mass, momentum, and energy conservation equations to simulate coal gasification and combustion. Coal particles at high temperatures, the heat transfer between the dispersed and fluid phases, and the resulting chemical reactions and heat transfer by radiation are illustrated in detail further on.

Over the past few years, comprehensive research has been devoted to gasification process and performance via CFD modeling [10-22]. Chen et al. [23] implemented a three-dimensional model to simulate a 200-ton, two-stage air-blown entrained type gasifier, developed for an IGCC process. The numerical analysis showed that turbulent fluctuations affected the volatiles and char-oxygen reactions and significantly influenced the temperature and gas composition. Furthermore, Chen et al. [24] also found that carbon conversion is independent of the devolatilization rate and less sensible to coal particle size, but it is sensitive to the heterogeneous char-oxygen, char-CO_2, and char-steam reaction kinetics.

Since 2005, numerous attempts have been made by the research team, the Energy Conversion & Conservation Center (ECCC) at the University of New Orleans [25-31], to develop a gasification numerical model through ANSYS/FLUENT. The model is based on a two-stage, entrained-flow gasifier following the geometry and input parameters of Bockelie et al. [13] and Chen et al. [23]. They compared different simulated models and concluded that: (1) the instantaneous gasification model predicts the reactions occurring faster and finishing more quickly than the finite-rate model, which involves the gas-solid reactions; (2) the instantaneous gasification model can provide an overall evaluation on gasifier performances, but cannot adequately capture the local gasification process inside the gasifier; (3) the water-shift rate plays an important role on predicting syngas composition, and the result of using a fast water-shift rate is close to that of using the global equilibrium method. They have also investigated various operating conditions; the results are summarized as follows [26]: (1) coal powder feedstocks tend to generate more CO and a higher outlet temperature than coal slurries with equivalent coal mass flow rates; (2) the exit gases of oxygen-blown gasifiers have higher mole concentrations of CO_2 and CO than air-blown gasifiers; (3) for the two-stage gasifier they studied, one-stage operation yields higher H_2, CO, and CH_4 concentrations than if a two-stage operation is used, but with a lower syngas heating value.

Since 2009 INER has been devoted to the field of gasification numerical modeling via the CFD software, FLUENT [3, 4, 32]. The instantaneous gasification model was used to investigate the gasification process of the E-Gas type gasifier. The effect of the coal slurry concentration has been analyzed. A lower Coal/H_2O ratio is preferred over high Coal/H_2O to produce H_2 with a lower exit syngas temperature, while a higher Coal/H_2O is better to produce more CO with a higher exit temperature. The overall results revealed that the instantaneous gasification model can quickly obtain preliminary results of coal combustion and gasification in a two-stage entrained-flow gasifier [3].

Gasification Theory

Gasification occurs due to an insufficient supply of oxidant, and the amount of supplied oxygen for coal gasification is usually from 1/3 to 1/5 of that for complete combustion. It is a process that coverts various carbon-based fuels to synthetic gas composed of CO, H_2, CO_2, H_2O, CH_4 and so forth. In general, coal gasification is categorized for three main steps: (1) devolatilization, (2) volatile combustion and thermal cracking, (3) char combustion and gasification (or char oxidation). The volatiles are polymeric compounds, consisting of C, H, O, N, S and ash, and in this paper the assumed volatiles chemical formula, $C_xH_yO_z$, is used in the volatiles reaction. Basically, the coal gasification process can be divided to heterogeneous reactions and homogenous reactions which are described below [8]:

Heterogeneous reactions

The overall reaction of gasification starts with incomplete combustion as:

$$C(s) + \tfrac{1}{2}O_2 \rightarrow CO, \Delta H_R^\circ = -110.5 MJ/kmol \qquad \text{(R1)}$$

This reaction is an exothermic reaction, and the produced CO will continually react rapidly with free oxygen to produce CO_2.

Due to the richness of fuel in the gasifier, a much slower endothermic CO-gasification (Boudouard) reaction may occur:

$$C(s) + CO_2 \rightarrow 2CO, \Delta H_R^\circ = +172.0 MJ/kmol \qquad \text{(R2)}$$

In order to generate more H_2 to increase heating value, steam is injected into the gasifier to react with carbon through the steam-gasification reaction:

$$C(s) + H_2O \rightarrow CO + H_2, \Delta H_R^\circ = +131.4 MJ/kmol \quad \text{(R3)}$$

Homogenous reactions

The reaction rates of the homogenous reaction are much faster than that of the heterogeneous reactions. The CO from the three above heterogeneous reactions will react quickly with oxygen to produce CO_2

$$CO + \tfrac{1}{2}O_2 \rightarrow 2CO_2, \Delta H_R^\circ = -283.1 MJ/kmol \quad \text{(R4)}$$

Due to the addition of steam, CO will go through the slightly exothermic water-gas-shift (WGS) reaction and this reaction rate has a strong influence on the H_2/CO ratio in the exit syngas composition:

$$CO + H_2O \leftrightarrow CO_2 + H_2, \Delta H_R^\circ = -41.0 MJ/kmol \quad \text{(R5)}$$

The volatiles are modeled to thermally crack to four species, CO, H_2, CH_4 and C_6H_6 [25]:

$$CH_{2.761}O_{0.264} \rightarrow 0.3585H_2 + 0.264CO + 0.436CH_4 + 0.05C_6H_6 \quad \text{(R6)}$$

CH_4 and C_6H_6 are further modeled being gasified with oxygen into CO and H_2:

$$CH_4 + \tfrac{1}{2}O_2 \rightarrow CO + 2H_2 \quad \text{(R7)}$$

$$C_6H_6 + 3O_2 \rightarrow 6CO + 3H_2 \quad \text{(R8)}$$

2. NUMERICAL SCHEME

In the numerical procedure, the 3-D, steady-state Navier-Stokes equations are solved in an Eulerian-Lagrangian frame of reference. All the coal particles are treated as a discrete, secondary phase dispersed in the continuous phase via the Discrete Phase Model (DPM) with the stochastic tracking to consider the turbulent dispersion effect. The P1 radiation model is used, and the gravitational force is considered in the modeling. The standard *k-ε* model is used to capture the turbulence flow. The species transport equations are solved through the Finite-Rate/Eddy-Dissipation Model. In this model, both the finite rate and the eddy-dissipation rate are used and compared, and the slower rate is selected to compute the continuous phase reactions.

Governing equations

The equation for conservation of mass is:

$$\nabla \cdot (\rho \vec{v}) = S_m \quad (1)$$

The source term S_m is the additional mass including the vaporization of water droplets and the devolatilization of coal particles added to the continuous phase from the dispersed second phase flow.

The momentum conservation equation is:

$$\nabla \cdot (\rho \vec{v}\vec{v}) = -\nabla p + \nabla \cdot (\bar{\bar{\tau}}) + \rho\vec{g} + \vec{F} \quad (2)$$

where p is the static pressure, $\bar{\bar{\tau}}$ is the stress tensor, and $\rho\vec{g}$ and $\vec{F}$ are the gravitational body force and external body forces (e.g. that arise from interaction with the dispersed phase), respectively.

The stress tensor $\bar{\bar{\tau}}$ is given by

$$\bar{\bar{\tau}} = \mu\left[\left(\nabla\vec{v} + \nabla\vec{v}^T\right) - \frac{2}{3}\nabla\cdot\vec{v}I\right] \quad (3)$$

where μ is the molecular viscosity, I is the unit tensor, and the second term on the RHS is the effect of volume dilation.

The energy conservation equation is:

$$\frac{\partial}{\partial x_i}\left(\rho\overline{u}_i h\right) = \frac{\partial}{\partial x_i}\left(K\frac{\partial T}{\partial x_i}\right) + S_{ph} \quad (4)$$

where the second term on the RHS is the source term for particle-gas heat transfer, evaporation energy (latent heat), the radiation energy, and reaction heat.

Turbulence model

The turbulence kinetic energy, k, and its rate of dissipation, ε, are obtained from the following standard *k-ε* transport equations:

$$\frac{\partial}{\partial x_i}(\rho k u_i) = \frac{\partial}{\partial x_j}\left[\left(\mu + \frac{\mu_t}{\sigma_k}\right)\frac{\partial k}{\partial x_j}\right] + G_k - \rho\varepsilon \quad (5)$$

and

$$\frac{\partial}{\partial x_i}(\rho\varepsilon u_i) = \frac{\partial}{\partial x_j}\left[\left(\mu + \frac{\mu_t}{\sigma_\varepsilon}\right)\frac{\partial \varepsilon}{\partial x_j}\right] + C_{1\varepsilon}\frac{\varepsilon}{k}G_k - C_{2\varepsilon}\rho\frac{\varepsilon^2}{k} \quad (6)$$

In these equations, G_k represents the generation of turbulence kinetic energy due to the mean velocity gradients. σ_k and σ_ε are the turbulent Prandtl numbers for k and ε. The turbulent (or eddy) viscosity, μ_t, is computed by combining k and ε as follows:

$$\mu_t = \rho C_\mu \frac{k^2}{\varepsilon} \quad (7)$$

the empirical model constants are $C_{1\varepsilon}$ = 1.44, $C_{2\varepsilon}$ = 1.92, C_μ = 0.09, σ_k = 1.0, σ_ε= 1.3 [33].

Discrete phase

In the Largrangian approach, each particle is tracked. The force balance on the discrete phase particles can be written as

$$\frac{du_p}{dt} = F_D(u-u_p) + \frac{g_x(\rho_p-\rho)}{\rho_p} \tag{8}$$

where $F_D(u-u_p)$ is the drag force per unit particle mass:

$$F_D = \frac{18\mu}{\rho_p d_p^2}\frac{C_D R_e}{24} \tag{9}$$

$$Re = \frac{\rho d_p |u_p - u|}{\mu} \tag{10}$$

where u is the fluid phase velocity, u_p is the particle velocity, μ is the molecular viscosity of the fluid, ρ is the fluid density, ρ_p is the particle density, and d_p is the diameter of the particle which is treated as a spherical shape. Re is the relative Reynolds number.

The track of the particle is evaluated by the instantaneous velocity, which is related to the mean velocity and the fluctuating velocity as:

$$u^* = \bar{u} + u' \tag{11}$$

where the fluctuating velocity in Eq. (11) is defined by the stochastic discrete random walk model.

The relationships for calculating the burning rate of the char particles are presented and discussed in detail by Smith [34]. The reaction rate $\overline{R}$ (kg/s) of particle surface species depletion as a particle undergoing an endothermic reaction in the gas phase is given as:

$$\overline{R} = A_p \eta Y R \tag{12}$$

$$R = R_{kin}\left(p_n - \frac{R}{D}\right)^N \tag{13}$$

where A_p is the particle surface area (m^2), Y is the mass fraction of surface species in the particle, η is the effectiveness factor (dimensionless), R is the rate of particle surface species reaction per unit area (kg/m^2-s), p_n is the bulk partial pressure of the gas phase species (Pa), D is the diffusion rate coefficient for the reaction, R_{kin} is the kinetic rate of reaction (units vary), and N is the apparent order of reaction. The kinetic rate of reaction r is defined as:

$$R_{kin} = AT^n e^{-(E/RT)} \tag{14}$$

When the coal slurry particle is injected into the gasifier, the water is assumed to be atomized to small droplets and undergoes evaporation. The rate of vaporization is controlled by concentration difference between the surface and gas streams, and the corresponding mass change rate of the droplet can be given by:

$$\frac{dm_p}{dt} = \pi d^2 k_c (C_s - C_\infty) \tag{15}$$

where k_c is the mass transfer coefficient and C_s is the concentration of the vapor at the particle's surface, which is evaluated by assuming that the flow over the surface is saturated. C_∞ is the vapor concentration of the bulk flow, obtained by solving the transport equations. The value of k_c can be calculated from empirical correlations by [35, 36]:

$$Sh_d = \frac{k_c d}{D} = 2.0 + 0.6\, Re_d^{0.5}\, Sc^{0.33} \tag{16}$$

where Sh is the Sherwood number, Sc is the Schmidt number (defined as v/D), D is the diffusion coefficient of vapor in the bulk flow. Re_d is the Reynolds number, defined as uv/D, u is the slip velocity between the droplet and the gas and D is the droplet diameter.

When the droplet temperature reaches the boiling point, the following equation can be used to evaluate its evaporation rate [37]:

$$\frac{dm_d}{dt} = \pi d^2 \left(\frac{\lambda}{d}\right)\left(2.0 + 0.46\,\mathrm{Re}_d^{0.5}\right)\ln\left(1 + C_p(T_\infty - T)/h_{fg}\right)/C_p \tag{17}$$

The energy equation for the particle accounts for convection, radiation, devolatilization, and surface reactions, is given as:

$$m_p c_p \frac{dT_p}{dt} = hA_p(T_\infty - T_P) + \varepsilon_p A_p \sigma\left(\theta_R^4 - T_p^4\right) + \frac{dm_p}{dt} h_{fg} - f_h \frac{dm_p}{dt} H_{reac} \tag{18}$$

where m_p and T_p are the particle mass and particle temperature, respectively. θ_R is the radiating temperature, defined as:

$$\theta_R = (G/4\sigma)^{1/4} \tag{19}$$

and G is the incident radiation, which is related to the radiative intensity as:

$$G = \int_0^{4\pi} I d\Omega \tag{20}$$

The radiation in the gasifier is described by the P1 model [38]. The convection coefficient between the particle and the gaseous flow field is evaluated by the empirical relation proposed by Ranz and Marshall [35] as:

$$N_u = \frac{hd_p}{k} = 2.0 + 0.6\,\mathrm{Re}_d^{1/2}\,\mathrm{Pr}^{1/3} \tag{21}$$

Devolatilization

The devolatilization reaction of the coal particle is described by the two-competing-rates model proposed by Kobayashi [39] as:

$$R_1 = A_1 e^{-(E_1/RT_p)} \tag{22}$$

$$R_2 = A_2 e^{-(E_2/RT_p)} \tag{23}$$

These two kinetic rates are used as a weight function by an expression for devolatilization as:

$$\frac{m_v(t)}{(1-f_{\omega,0})m_{p,0}-m_a} = \int_0^t (\alpha_1 R_1 + \alpha_2 R_2) \exp\left(-\int_0^t (R_1+R_2)dt\right)dt \tag{24}$$

where α_1 and α_2 are yield factors, f_ω is the mass fraction of moisture, m_p is the mass of particle, and m_a is the mass of ash. The value of the constants are $A_1 = 2\times10^5$, $A_2 = 1.3\times10^7$, $E_1 = 1.046\times10^8$ J/kg mol, and $E_2 = 1.67\times10^8$ J/kg mol.

As the volatiles diffuse out of the coal particle, the heterogeneous reactions on the particle surface occur. Those particle surface reactions are described by the implicit relations of Smith et al. [34] as:

$$\overline{R}_{k,r} = A_p \eta_r Y_k R_{k,r} \tag{25}$$

$$R_{k,r} = R_{kin,r}\left(p_n - \frac{R_{k,r}}{D_{0,r}}\right)^{N_r} \tag{26}$$

$$R_{kin,r} = A_r T^{n,r} e^{-(E_r/RT)} \tag{27}$$

Chemical reaction

The conservation equation of the species is in the following general form:

$$\nabla\cdot(\rho\vec{\upsilon}Y_i) = -\nabla\cdot\vec{J}_i + R_i + S_i \tag{28}$$

where R_i is the net rate of production of species i by chemical reaction and S_i is the rate of mass creation by addition from the dispersed phase sources. $\vec{J}_i$ is the diffusion flux of species i, which arises due to the gradients in concentration and temperature.

The source term for species i due to all reactions is computed as the sum of the Arrhenius reaction sources over the N_R reactions that the species participate in:

$$R_i = M_{w,i}\sum_{r=1}^{N_R}\hat{R}_{i,r} \tag{29}$$

where $M_{w,i}$ is the molecular weight of species i and $\hat{R}_{i,r}$ is the Arrhenius molar rate of production/consumption of species i in reaction r.

The Finite-rate/Eddy-dissipation-rate model computes both Arrhenius rates and turbulent mixing rates, and the smaller one is chosen for the homogeneous reactions. While only finite rates are used for the heterogeneous reactions.

Finite-rate/Eddy-dissipation-rate model

Arrhenius rate:

$$\hat{R}_{i,r} = (\nu''_{i,r}-\nu'_{i,r})\left(k_{f,r}\prod_{j=1}^{N}[C_j]^{\eta'_{j,r}} - k_{b,r}\prod_{j=1}^{N}[C_j]^{\eta''_{j,r}}\right)$$
$$k_{f,r} = A_r T^n \exp(-E_r/RT) \tag{30}$$
$$k_{b,r} = \frac{k_{f,r}}{K_k}$$

where $\nu'_{i,r}, \nu''_{i,r}$ are the reactant and product stoichiometric coefficients, respectively, $\eta'_{j,r}, \eta''_{j,r}$ are the rate exponents for reactant j and product j, respectively, in reaction r, n is the temperature exponent of reaction r, E_r is the activation energy, R is the universal gas constant, A_r is the pre-exponential factor, C_j is the molar concentration of species j, and K_k is the equilibrium constant.

Eddy-dissipation rate:

$$R_{i,r} = min(R_{i,r}^{(R)}, R_{i,r}^{(P)})$$
$$R_{i,r}^{(R)} = \nu'_{i,r}M_i A\rho\frac{\varepsilon}{k}\left(\frac{Y_R}{\nu'_{R,r}M_R}\right) \tag{31}$$
$$R_{i,r}^{(P)} = \nu''_{i,r}M_i AB\rho\frac{\varepsilon}{k}\frac{\sum_P Y_P}{\sum_j^N \nu''_{j,r}M_j}$$

where Y_R and Y_P are the mass fractions of species, A is the Magnussen constant for reactants (4.0), B is the Magnussen constant for products (0.5), M is the molecular weight, and the R and P subscripts are the reactants and products.

The global gasification reaction rates used in this study are listed in Table 1 [27].

Table 1 Global reaction rate constants in this study

Reaction	n	A_r	E_r (J/kmol)
$C_{(s)} + 1/2O_2 \rightarrow CO$	0	0.052 kg/m^2 Pa$^{-0.5}$	6.10E+07
$C_{(s)} + CO_2 \rightarrow 2CO$	0	0.0732 kg/m^2 Pa$^{-0.5}$	1.125E+08
$C_{(s)} + H_2O \rightarrow CO + H_2$	0	0.0782 kg/m^2 Pa$^{-0.5}$	1.15E+08
$CO + 1/2O_2 \rightarrow CO_2$	0	2.20E+12	1.67E+08
$CH_{2.761}O_{0.264} \rightarrow 0.3585H_2 + 0.264CO + 0.436CH_4 + 0.05C_6H_6$	0	Eddy-dissipation rate only	
$C_6H_6 + 3O_2 \rightarrow 6CO + 3H_2$	0		
$CH_4 + 1/2O_2 \rightarrow CO + 2H_2$	0		
$CO + H_2O \rightarrow CO_2 + H_2$	0	2.75E+02	8.38E+07

3. MODEL DESCRIPTION

Computational model

Most geometric dimensions of the E-Gas like gasifier in this study are referred to the NETL's published document [40]. Part of the dimensions, including injector size, throat height and diameter, are estimated. The sketch of the computational model is shown in Fig. 1. The E-Gas like gasifier is divided to two sections, consisting of a horizontal vessel (width: 8m; diameter: 2m) and a vertical cylinder (height: 10m, diameter: 1.6m). There are two injectors opposed to each other, located on each end of the horizontal section at a height of 1m. Only one injector is located in the throat region at a height of 3.6m. All the oxidant consisting of 95% O_2 mixed with 5% N_2 is fed into the 1st stage section. The coal slurry is injected in the two-stage arrangement with 78% of the coal slurry being fed into the 1st stage section, and the remaining coal slurry being supplied to the 2nd stage section.

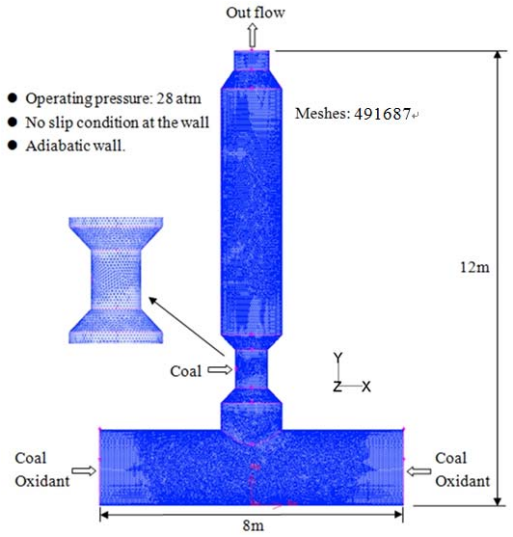

Fig. 1 Schematic of computational model

Four grids (0.12, 0.31, 0.49, and 1.05 million cells) are examined for the grid independent test, and the results are shown in Table 2**.** The differences of the species between the cases of 0.49M and 1.05M are less than 1%, and the difference of outlet temperature between the two cases is less than 3%. Since the objective of this study is to develop the finite-rate gasification model and examine the global gasification behavior rather than to seek very accurate solutions, the 0.49M grid is hence used for further studies.

Table 2 Outlet results of the grid independent test

Cell no.		0.12M	0.31M	0.49M	1.05M
Mole Fraction (%)	CO	38.26	38.64	38.59	38.36
	H_2	23.21	23.3	23.26	22.69
	CO_2	11.86	11.49	11.56	11.76
	H_2O	17.39	17.45	17.43	17.90
Temperature (K)		1876	1863	1865	1910

Boundary Condition

Illinois #6 coal is used in this study, and its compositions of proximate and ultimate analyses are shown in Table 3.

In order to simplify the computational model, the masses of Cl and S are lumped into N_2 and treated as a gas phase along with the oxidant in the model. The treatment of the ash transformation (i.e. transformation to slag) is neglected, and, hence, SiO_2 is used as a gas species to represent ash in the model. The total slurry mass flow rate is 39.7 kg/s, and the total oxidant mass flow rate is 22.9 kg/s. The operating pressure is 28 atm. Refractory brick is used in the real case of the E-Gas gasifier; however the properties of the material is not known, and therefore, in this study, the wall is assumed to be adiabatic. The detailed inlet and boundary conditions of the base case are summarized in Table 4. The ratio of O_2/Coal is 0.918 and the coal slurry concentration is 0.67. The corresponding O/C and H_2O/C mass ratios are shown in Table 5.

The definitions of O_2/Coal and coal slurry concentration are:

$$O_2/Coal = \frac{mass\ of\ O_2}{mass\ of\ Coal\ (DAF)}$$

$$Coal\ slurry\ concentration = \frac{mass\ of\ Coal\ (MF)}{mass\ of\ Coal\ Slurry}$$

Table 3 Compositions of Illinois #6 coal

Proximate Analysis	Wt. %	Ultimate Analysis	Wt. %
Moisture	11.12	Moisture	11.12
Fixed Carbon	44.19	Carbon	63.75
Ash	9.70	Hydrogen	4.50
Volatiles	34.99	Nitrogen	1.25
Total	100	Chlorine	0.29
		Sulfur	2.51
		Ash	9.70
		Oxygen	6.88
		Total	100

Table 4 Boundary conditions

Inlet	Stage 1	Stage 2
$\dot{m}_{gas}$ (kg/s)	26.11	0.91
$\dot{m}_{coal}$ (kg/s)	20.13	5.68
$\dot{m}_{H_2O}$ (kg/s)	7.62	2.15
$T_{oxidant}$ (K)	411	-
$T_{coal\ slurry}$ (K)	450	450

Table 5 The corresponding O/C and H_2O/C mass ratio

O_2/Coal(DAF)	O/C	Coal slurry concentration	H_2O/C
0.918	1.1403	0.67	0.6867

4. RESULTS AND DISCUSSION

Base case description

Figure 2 shows the temperature contours on a vertical mid-plane and a horizontal plane. There are two main cold streams in the 1st stage section, indicating the low-temperature trace of the freshly injected coal-water slurry and oxidant. A high temperature region occurring in the 1st stage section indicates that most of exothermic reactions take place in the bottom horizontal cylinder, and the highest temperature in this region is about 3004K. Whereas in the 2nd stage section, an obvious temperature drop occurs after the 2nd stage burner, indicating that the endothermic gasification reactions dominate in this region under the oxidant-starved condition.

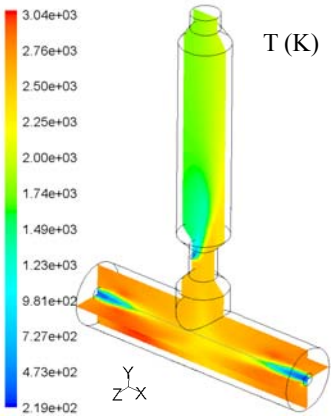

Fig. 2 Temperature contours of the base case

Figure 3 shows the mole fraction contours of the four major gas species, CO, H_2, CO_2, and H_2O, as well as the particle concentration and volatiles contours. The analysis will be made in the first and second stage separately.

In the 1st stage in the bottom cylinder --- First, as the coal particles are fed into the bottom cylinder, they absorb heat and undergo the evaporation and devolatilization process, which can be observed from the contours of H_2O and the volatiles. This endothermic process results in the low-temperature in the mid-core region near the inlets. In addition, a comparison of the contours of CO and CO_2 indicates that CO is first produced along the core of the mid-section of the bottom cylinder where two injection jets travel and meet. Then the CO_2 is produced surrounding the core of the CO-production region, shaped like a series of tori in the vertical cross-sectional contour views. This indicates that reaction R1 (oxidation of the solid carbon) is dominant along the mid-plane core region and CO combustion (R2) is the major reaction in the region surrounding the CO. The H_2 is produced near the inlet region and in the annular region wrapping around the mid-core region of high CO concentration possibly via the water shift reaction (R5). Since H_2 production gets higher near the middle region of the bottom cylinder, thermal cracking of the volatiles (R6, 7, and 8) is believed the cause of this result.

In the 2nd stage in the vertical cylindrical section --- The main purpose of the second stage is to maximize the gasification reactions (R2 and 3) without adding more oxidant to reduce the reactor temperature and to make the injectors and refractory wall last longer. This goal is clearly achieved as it can be seen from the significantly reduced temperature (Fig. 2) and the increased H_2 and CO distributions (Fig. 3) in the second stage. Furthermore, the occurrence of the active Boudouard and steam gasification reactions (R2 and 3) can be supported by quick consumptions of CO_2 and H_2O in the region near the second injection location in Fig. 3. After the height of 8m, the mole fraction of these four major product species reach the equilibrium state, in other words, the mole fraction of these species do not change with the height.

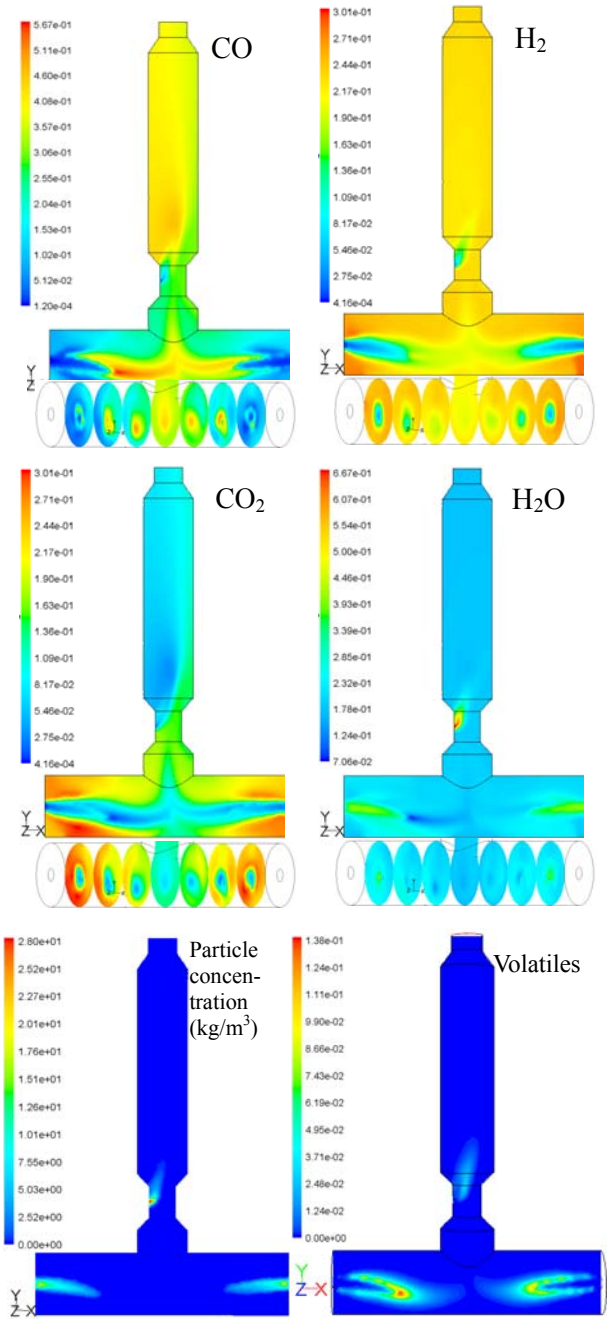

Fig. 3 Species mole fraction contour, particle concentration, and volatiles contour of base case

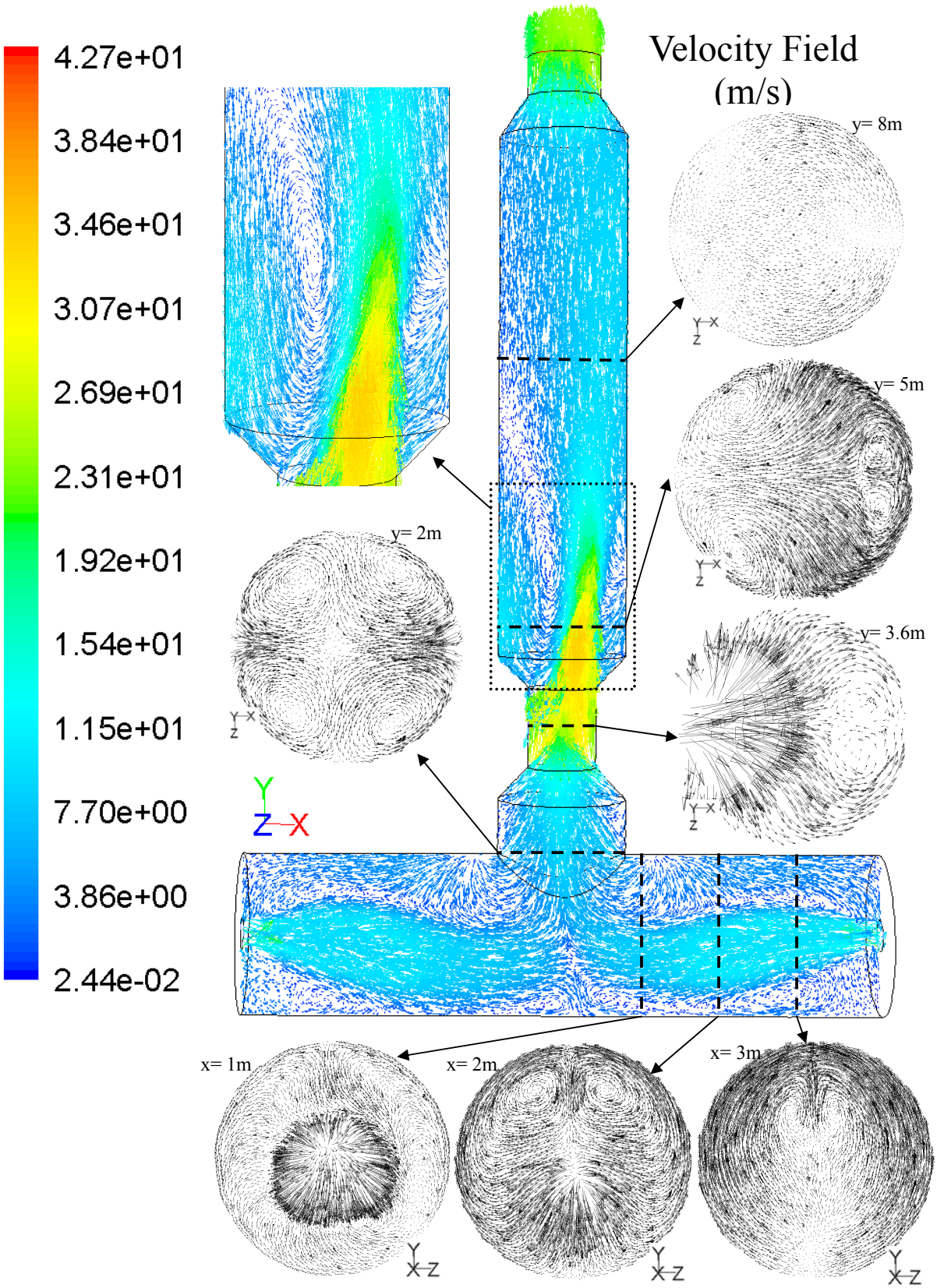

Fig. 4 Velocity vector of xy-plane and cross-section plane at different positions

Figure 4 shows the velocity vectors of the mid-plane. The overall flow motion shows that in the first stage in the bottom cylinder two strong streams consisting of fresh coal slurry and oxidant impinge against each other in the middle of the bottom cylinder and then flow upward to the second stage section. Due to the strongly lateral injection the upward stream deflects away from the 2nd stage injection and results in a large recirculation zone above the 2nd stage injector. This slow-moving recirculation zone occupies a portion of the gasifier like a blockage which reduces the effective area for the core flow to pass through. This leads to a longer residence time for the flow trapped in the recirculation zones but accelerates the core flow due to reduced effective through-flow area. The gas species trapped in the recirculation zone seems to extend the mixing time of gas species, but the reduced area separates the accelerated upward-stream from the recirculation zone and hence reducing the opportunities of species mixing. Only a small part of species in the recirculation zone experiences a good mixing, whereas the main upward stream does not. This would not be an ideal condition for gasification for that not all the species inside the gasifier have the sufficient time and space to proceed gasification.

Seven detailed views of velocity vectors of horizontal and vertical cross-section planes are also shown in Fig. 4. From the bottom cross-sectional view, it can be seen that there are two small vortices occurring above the main stream and then disappear near the center of the cylinder in the first stage. As the stream flows from the horizontal cylinder upward, four small vortices can be found in the left cross-sectional view and these vortices also disappear as the upward stream flows through the throat region.

The outlet syngas composition and temperature results are compared with the reference data of NETL report [40] in Table 6. Except for H_2O which has a 6.52 percentage point difference, the differences of all other outlet gas species are below 3 percentage points.

Table 6 Exit syngas temperature and compositions of base case

Parameters	Base case	Reference [40]
Exit temperature (K)	1865	-
Components at exit:	**Mole fraction (%)**	**Mole fraction (%)**
CO	38.59	35.90
H_2	23.26	22.90
CO_2	11.56	12.20
H_2O	17.43	23.90
N_2	3.00	2.00
CH_4	4.01	1.70

Effect of O_2/Coal ratio

Table 7 shows the effects of the O_2/Coal ratio on the gasification results at a fixed coal slurry concentration feed rate. Five O_2/Coal ratios, which are altered by changing the oxidant flow rate only, are conducted for comparison in this section. When more oxidant is fed into the gasifier, the exit temperature and mole concentration of CO_2 increases significantly as expected and the mole concentration of CO decreases due to more complete combustion occurring. Besides, both the syngas higher heating value (HHV) and cold gas efficiency (CGE) decrease due to the increase of CO_2 and decrease of CO. It represents that the increased O_2/Coal ratio results in more combustion to produce heat but a poorer gasification performance for producing fuels.

Table 7 Effect of O_2/Coal ratio on exit temperature and compositions

O_2/Coal (DAF)	0.8	0.85	0.92	0.95	1.00
Exit temperature (K)	1543	1685	1865	1957	2086
Components at exit:	**Mole fraction (%)**				
CO	42.98	41.09	38.59	36.9	35.34
H_2	23.39	23.13	23.26	23.5	23.66
CO_2	7.15	9.04	11.56	13.18	14.79
H_2O	16.83	17.2	17.43	17.5	17.55
Syngas HHV (MJ/kg)	11.79	11.22	10.49	10.06	9.62
CGE (%)	86.69	84.27	81.00	78.62	76.65

Effect of coal slurry concentration

In this part, the influence of coal slurry concentration (CSC) is examined. The results of three CSC values, 0.55, 0.67 and 0.75, are compared and shown in Table 8. As the CSC decreases, i.e. the amount of additional water increases under the same O_2/Coal ratio, the exit temperature and mole fraction of CO, H_2 and CO_2 decrease and the amount of H_2O vapor increases. This result is not consistent with the common intuition, because by adding more water (or reducing CSC), both H_2 and CO_2 are supposed to increase rather than decrease due to increased WGS reaction [41]. To search for an answer to the above result, attention has been placed on investigating the reaction rate of WGS.

The chemical rate of the WGS reaction in Table 1 used in this study is reduced from the original value of Jones and Lindstedt [42]. According to Silaen and Wang [27], the original value of WGS reaction rate with the pre-exponential factor of 2.75E+10 used in [42] was obtained under the condition when a catalyst was applied, and therefore, the pre-exponential factor of the reaction rate was reduced to 2.75E+02 when no catalyst is used to match some published syngas composition data from entrained-bed gasifiers. Therefore, a series of modified reaction rates have been tested in this part of the study and a new value of the pre-exponential factor, 2.75E+03, is found, giving a more reasonable result as shown in Table 9. Since adding water into the slurry will change the total volume and hence affect the mole fractions of species, just looking at the changes in mole fraction could be misleading: rather, the mass flow rates should be compared. Consequently, both the mole fraction and the exit mass flow rates of each species are listed in Table 9. It can also be seen in Table 9 that as the amount of additional water increases (i.e.

the CSC value decreases), the mass flow rates of H_2 and CO_2 increase, accompanied with reduced CO mass flow rate,.

However, due to the reason that only scant information on the reaction rate of the WGS reaction is revealed without using a catalyst under a typical operation condition in a entrained-bed gasifier as well as a lack of adequate gasification experimental data including the amount of water vapor immediately measured at the reactor exit of the gasifier before the cooling or gas-cleaning sections, no solid conclusion can be made on the model established in this study except it can certainly conclude that the WGS reaction rate has a major influence on predicting the gasification process.

Table 8 Exit syngas temperature and compositions of different CSC values using the WGS reaction rate with the pre-exponential factor of 2.75E+02

CSC	**0.55**	**0.67**	**0.75**
Exit temperature(K)	1555	1865	2098
Components at exit:	**Mole fraction (%)**		
CO	33.39	38.59	41.16
H_2	18.3	23.26	26.22
CO_2	9.31	11.56	13.47
H_2O	30.84	17.43	9.69
Components at exit:	**Mass flow rate (kg/s)**		
CO	30.46	30.26	29.64
H_2	1.20	1.31	1.36
CO_2	13.33	14.24	15.23
H_2O	18.09	8.79	4.49

Table 9 Exit syngas temperature and compositions of different CSC values using modified WGS reaction rate with the pre-exponential factor of 2.75E+03

CSC	**0.55**	**0.67**	**0.75**
Exit temperature(K)	1622	1915	2079
Components at exit:	**Mole fraction (%)**		
CO	21.55	27.36	34.76
H_2	30.64	35.29	33.89
CO_2	21.17	22.82	19.98
H_2O	18.64	5.67	1.81
Components at exit:	**Mass flow rate (kg/s)**		
CO	19.73	21.59	25.22
H_2	2.02	2.00	1.77
CO_2	30.43	28.29	22.74
H_2O	10.97	2.88	0.85

Effect of 1st-2nd stage fuel distribution

The original condition of the fuel distribution between the 1st and 2nd stages from the NETL's report [40] is 78% and 22% respectively. Two other fuel distribution ratios, 50%-50% and 100%-0%, are examined in this paper. Table 10 shows the gasification results on different fuel feeding conditions in terms of exit temperature and syngas compositions as well as their syngas high heating values (HHV) and cold gasification efficiency (CGE). The results show that as the amount of coal slurry in the first stage increases, the exit temperature and the mole concentration of H_2 and CO_2 increase, while the mole concentration of CO decreases.

Although the case of 78%-22% has a relatively higher syngas HHV and CGE, the differences between the three cases are too little to judge which one has the best gasification performance. The little difference between the three cases can be explained by the fact that the space inside the E-Gas gasifier is large enough to achieve equilibrium reactions, and hence the influence of fuel distribution on the gasification performance is less noticeable. Figure 5 shows the mass-weighted temperature and mole fraction distributions along the gasifier height on different fuel distribution conditions. From the figure, it can be seen that the differences in temperature, and CO and CO_2 concentrations are quite obvious in the range (from 0m to 4m) that the combustion reactions are more dominant. Due to the injection of fresh coal slurry in the 2nd stage injector, there are dramatic local changes of temperature and species mole fractions at 4m for the 50%-50% and 78%-22% cases. However, the differences converge at the exit.

Table 10 Gasification performance and exit syngas temperature and compositions under various fuel feeding conditions between the 1st and 2nd stages

1st-2nd stage fuel distribution	**50%-50%**	**78%-22% (base case)**	**100%-0% (one stage)**
Exit temperature (K)	1858	1865	1900
Components at exit:		**Mole fraction (%)**	
CO	39.90	38.59	37.27
H_2	21.87	23.26	24.65
CO_2	10.20	11.56	12.96
H_2O	18.94	17.43	16.14
Syngas HHV (MJ/kg)	10.46	10.49	10.45
CGE (%)	80.73	81.00	80.68

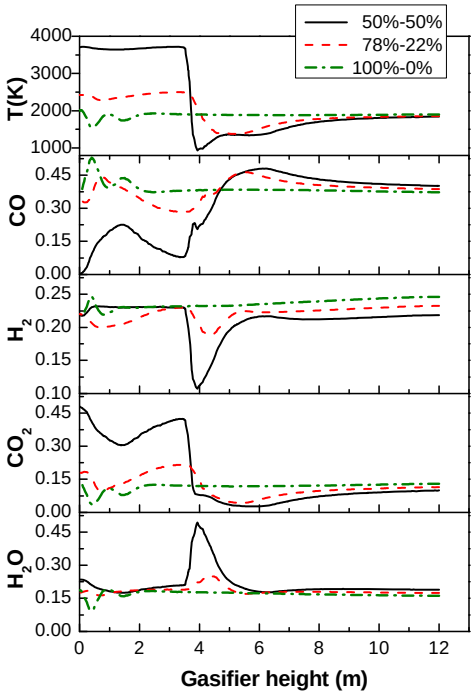

Fig. 5 Mass-weighted temperature and mole fraction distributions along the gasifier height on different fuel distribution conditions

5. CONCLUSION

A 3-D computational model has been established to simulate the coal combustion and gasification processes in a cross-type, two-stage, and entrained-flow gasifier based on the Conoco-Phillips/E-Gas model by replacing the previous instantaneous gasification model with the finite-rate model for heterogeneous reactions. The results of the base case show good agreement with the NETL's result. A series of parametric studies have been conducted. The results are summarized as follows:

- Effect of O_2/Coal ratio – The increased O_2/Coal ratio leads to higher exit temperature and CO_2 concentration, but lower CO concentration. Both the decreased syngas HHV and CGE indicate that the increased O_2/Coal ratio results in more combustion to generate heat, but poorer gasification performance to produce fuels.

- Effect of coal slurry concentration – As the coal slurry concentration increases (i.e. the amount of water in the slurry is reduced), the amount of H_2, CO_2, and H_2O decreases, while only the amount of CO increases. The results are found very sensitive to the WGS reaction rate. It will need more accurate WGS reaction rates under non-catalytic conditions and better gasification syngas data measured immediately at the reactor exit with water vapor information before the cooling section to help validate the prediction model.

- Effect of 1st-2nd stage fuel feeding distribution – As the amount of coal slurry mass flow in the first stage increases, the exit temperature and the mole concentrations of H_2 and CO_2 increase, while the mole concentration of CO decreases. The comprehensive comparison shows that the case of 78%-22% led to marginally higher syngas heating value and cold gas efficiency.

ACKNOWLEDGEMENT

This research was supported by a grant from INER (Institute of Nuclear Energy Research) program, Clean Carbon as Sustainable Energy (CaSE), under the frame work of National Energy Program (NEP) at National Science Council of Taiwan, ROC.

REFERENCE

[1] Bp, 2010, "Statistical Review of World Energy 2010," London, UK.
[2] Boe, 2010, "Energy Statistical Hand Book 2009," Taipei, Taiwan.
[3] Chyou, Y. P., Huang, C. B., Luan, Y. T., and Wang, T., 2010, "Numerical Simulation of Gasification Process in a Cross-Type Two-Stage Gasifier," 27th International Pittsburgh Coal Conference, Istanbul, Turkey.
[4] Huang, C. B., Chyou, Y. P., and Chen, P. C., 2010, "Preliminary Numerical Study of Entrained Flow Coal Gasifier," 20th Combustion Conference, Tainan, Taiwan.
[5] Wen, C. Y., and Chaung, T. Z., 1979, "Entrainment Coal Gasification Modeling," Industrial & Engineering Chemistry Process Design and Development, 18: 684-695.
[6] Douglas Smoot, L., 1984, "Modeling of Coal-Combustion Processes," Progress in Energy and Combustion Science, 10: 229-267.
[7] Eaton, A. M., Smoot, L. D., Hill, S. C., and Eatough, C. N., 1999, "Components, Formulations, Solutions, Evaluation, and Application of Comprehensive Combustion Models," Progress in Energy and Combustion Science, 25: 387-436.
[8] Smoot, L. D., and Smith, P. J., 1985, *Combustion and Gasification of Coal,* Plenum Press, NY.
[9] Hill, S. C., and Smoot, L. D., 1993, "A Comprehensive Three-Dimensional Model for Simulation of Combustion Systems. Pcgc-3," Energy & Fuels, 7: 874-883.
[10] Fletcher, D. F., Haynes, B. S., Christo, F. C., and Joseph, S. D., 2000, "A Cfd Based Combustion Model of an Entrained Flow Biomass Gasifier," Applied Mathematical Modelling, 24: 165-182.
[11] Chen, C., Horio, M., and Kojima, T., 2001, "Use of Numerical Modeling in the Design and Scale-up of Entrained Flow Coal Gasifiers," Fuel, 80: 1513-1523.
[12] Choi, Y. C., Li, X. Y., Park, T. J., Kim, J. H., and Lee, J. G., 2001, "Numerical Study on the Coal Gasification Characteristics in an Entrained Flow Coal Gasifier," Fuel, 80: 2193-2201.
[13] Bockelie, M. J., Denison, M. K., Chen, Z., Linjewile, T., Senior, C. L., F., S. A., and Holt, N., 2002, "Cfd Modeling for Entrained Flow Gasifiers," Gasification Technologies Conference, San Francisco, CA.
[14] Vicente, W., Ochoa, S., Aguillón, J., and Barrios, E., 2003, "An Eulerian Model for the Simulation of an Entrained

Flow Coal Gasifier," Applied Thermal Engineering, 23: 1993-2008.
[15] Stephen, E. Z., and Guenther, C., 2005, "Gasification Cfd Modeling for Advanced Power Plant Simulations," National Energy Technology Laboratory, Morgantown, WV 26507-0880, USA.
[16] Shi, S. P., Zitney, S. E., Shahnam, M., Syamlal, M., and Rogers, W. A., 2006, "Modelling Coal Gasification with Cfd and Discrete Phase Method," Journal of the Energy Institute, 79: 217-221.
[17] Watanabe, H., and Otaka, M., 2006, "Numerical Simulation of Coal Gasification in Entrained Flow Coal Gasifier," Fuel, 85: 1935-1943.
[18] Slezak, A. A. J., 2008, "Modeling of Particle Trajectories of Coal Size and Density Fractions in a Gasifier," Ph.D. thesis, West Virginia, Morgantown.
[19] Ajilkumar, A., Sundararajan, T., and Shet, U. S. P., 2009, "Numerical Modeling of a Steam-Assisted Tubular Coal Gasifier," International Journal of Thermal Sciences, 48: 308-321.
[20] Hernandez, J. J., Aranda-Almansa, G., and Bula, A., 2010, "Gasification of Biomass Wastes in an Entrained Flow Gasifier: Effect of the Particle Size and the Residence Time," Fuel Processing Technology, 91: 681-692.
[21] Slezak, A., Kuhlman, J. M., Shadle, L. J., Spenik, J., and Shi, S., 2010, "Cfd Simulation of Entrained-Flow Coal Gasification: Coal Particle Density/Size Fraction Effects," Powder Technology, 203: 98-108.
[22] Ni, J., Yu, G., Guo, Q., Dai, Z., and Wang, F., 2011, "Modeling and Comparison of Different Syngas Cooling Types for Entrained-Flow Gasifier," Chemical Engineering Science, 66: 448-459.
[23] Chen, C., Horio, M., and Kojima, T., 2000, "Numerical Simulation of Entrained Flow Coal Gasifiers. Part I: Modeling of Coal Gasification in an Entrained Flow Gasifier," Chemical Engineering Science, 55: 3861-3874.
[24] Chen, C., Horio, M., and Kojima, T., 2000, "Numerical Simulation of Entrained Flow Coal Gasifiers. Part Ii: Effects of Operating Conditions on Gasifier Performance," Chemical Engineering Science, 55: 3875-3883.
[25] Silaen, A., and Wang, T., 2010, "Effect of Turbulence and Devolatilization Models on Coal Gasification Simulation in an Entrained-Flow Gasifier," International Journal of Heat and Mass Transfer, 53: 2074-2091.
[26] Silaen, A., and Wang, T., 2010, "Investigation of the Coal Gasification Process under Various Operating Conditions inside a Two-Stage Entrained Flow Gasifier," 27th International Pittsburgh Coal Conference, Istanbul, Turkey.
[27] Silaen, A., and Wang, T., 2009, "Comparison of Instantaneous, Equilibrium, and Finite-Rate Gasification Models in an Entrained-Flow Coal Gasifier," 26th International Pittsburgh Coal Conference, Pittsburgh, USA.
[28] Silaen, A., and Wang, T., 2008, "Effects of Turbulence and Devolatilization Models on Gasification Simulation," 25th International Pittsburgh Coal Conference, Pittsburgh, USA.
[29] Silaen, A., and Wang, T., 2006, "Part-Load Simulations and Experiments of a Small Coal Gasifier," 23rd International Pittsburgh Coal Conference, Pittsburgh, PA, USA.
[30] Silaen, A., and Wang, T., 2006, "Effects of Fuel Injection Angles on Performance of a Two-Stage Coal Gasifier," 23rd International Pittsburgh Coal Conference, Pittsburgh, USA.
[31] Silaen, A., and Wang, T., 2005, "Simulation of Coal Gasification inside a Two-Stage Gasifier," 22nd International Pittsburgh Coal Conference, Pittsburgh, PA, USA.
[32] Chen, M. H., Jiang, T. L., Chyou, Y. P., and Huang, C. B., 2010, "Numerical Simulation Analyses of an Entrained-Bed Gasification Reactor," 27th International Pittsburgh Coal Conference, Istanbul, Turkey.
[33] Launder, B. E., and Spalding, D. B., 1972, *Lectures in Mathematical Models of Turbulence,* Academic Press, London.
[34] Smith, I. W., 1982, "The Combustion Rates of Coal Chars: A Review," Nineteenth Symposium (International) on Combustion, 19: 1045-1065.
[35] Ranz, W. E., and Marshall, W. R., 1952, "Evaporation from Drops. Part 1," Chemical Engineering Progress, 48: 141-146.
[36] Ranz, W. E., and Marshall, W. R., 1952, "Evaporation from Drops. Part 2," Chemical Engineering Progress, 48: 173-180.
[37] Kuo, K. K., 1986, *Principles of Combustion,* John Wiley and Sons, New York.
[38] Cheng, P., 1964, "Two Dimensional Radiating Gas Flow by a Moment Method," AIAA, 2: 1662-1664.
[39] Kobayashi, H., Howard, J. B., and Sarofim, A. F., 1977, "Coal Devolatilization at High Temperatures," Symposium (International) on Combustion, 16: 411-425.
[40] Zitney, S. E., 2005, "Cape-Open Integration for Advanced Process Engineering Co-Simulation," National Energy Technology Laboratory, Morgantown, WV.
[41] Liu, K., Song, C., and Subramani, V., 2010, *Hydrogen and Syngas Production and Purification Technologies,* John Wiley & Sons, Inc., Hoboken, New Jersey.
[42] Jones, W. P., and Lindstedt, R. P., 1988, "Global Reaction Schemes for Hydrocarbon Combustion," Combustion and Flame, 73: 233-249.